

Uncertainties from metrology in the integrated luminosity measurement with the updated design of the very forward region of a detector at CEPC

Ivan Smiljanić¹, Ivanka Božović², and Goran Kačarević³

¹ *Vinca Institute of Nuclear Sciences - National Institute of the Republic of Serbia, University of Belgrade, M. Petrovica Alasa 12-14, Belgrade, Serbia*

**E-mail: i.smiljanic@vin.bg.ac.rs*

² *Vinca Institute of Nuclear Sciences - National Institute of the Republic of Serbia, University of Belgrade, M. Petrovica Alasa 12-14, Belgrade, Serbia*

³ *Vinca Institute of Nuclear Sciences - National Institute of the Republic of Serbia, University of Belgrade, M. Petrovica Alasa 12-14, Belgrade, Serbia*

.....
 At an e^+e^- collider machine-detector interface includes, among others, a calorimeter dedicated for precision measurement of the integrated luminosity at a per mill level or better. Usually, such a device is placed at the outgoing beams, to keep the spatial symmetries of the head-on collisions at accelerators with a non-zero crossing angle. At CEPC it is currently proposed that the luminometer is placed on the z-axis. We review a feasibility of precision measurement of the integrated luminosity at the Z^0 pole, from the point of view of systematic effects arising from metrology uncertainties, either concerning the luminometer position and alignment or the beam properties, with the luminometer centered around the z-axis.

1 Introduction

To meet precision requirements of the CEPC physics program, relative uncertainty of the integrated luminosity measurement should be of order of 10^{-4} at the Z^0 pole [1]. The method of integrated luminosity measurement at CEPC, as well as the machine parameters, detector concept, machine-detector interface (MDI) and physics performance, is described in [1]. A distinctive feature of the current MDI design at CEPC is that the luminometer is proposed to be placed at the z-axis. Although the impact of metrology on the integrated luminosity measurement at CEPC has been studied in [2] with the luminometer conventionally placed at the outgoing beams (s-axis), it is worth revisiting for the newly proposed geometry, since the integrated luminosity precision critically depends on the luminometer's position, as well as on the way of counting.

In this paper, we review the potential impact of locating the luminometer around the z-axis on uncertainties associated with measuring integrated luminosity. These uncertainties stem from mechanical factors like positioning and alignment of the luminometer and the fact that the beam properties are known within some margins. These effects are collectively referred to as metrology. Additionally, we examined the performance of different Bhabha counting methods, including the LEP-style asymmetric counting [3], typically utilized to mitigate systematic biases arising from asymmetries between the left and right detector halves.

The paper is organized as follows: in Section 2 we discuss the current layout of the very forward region of CEPC. In Section 3 we review the impact of detector manufacturing, positioning and alignment (Section 3.1), as well as the impact of uncertainties of the knowledge of the beam properties (asymmetry of beam energies, beam energy spread - BES and beam synchronization) in section 3.2. Concluding discussion is given in Section 4.

2 Forward region at CEPC

The MDI region of CEPC covers the area of 6 m from the interaction point (IP) in both directions, along the z-axis. The accelerator components inside the detector without shielding are within a conical space with an opening angle of 118 mrad. The crossing angle in the horizontal plane between the colliding beams at the IP is 33 mrad. The final focus length of colliding beams is 2.2 m [1]. It is proposed that the luminometer at CEPC should be placed at 950 mm distance from the interaction point, covering the polar angle region between 30 mrad and 105 mrad, which corresponds to the luminometer aperture of 28.5 mm for the inner radius and 100 mm for the outer. The fiducial volume of luminometer should

be between 53 mrad and 79 mrad. The luminometer will be placed half way to the tracking volume longitudinally. The layout of the MDI region at CEPC is illustrated in Fig. 1 [2]. Shower leakage from the outer edge of the luminometer has been studied and proven to be negligible after absorption by a 5 mm iron filter positioned around the luminometer [1]. However, this has been done under assumption that the luminometer will be placed around the outgoing beam and it is yet to be proven for the luminometer placed around the z-axis.

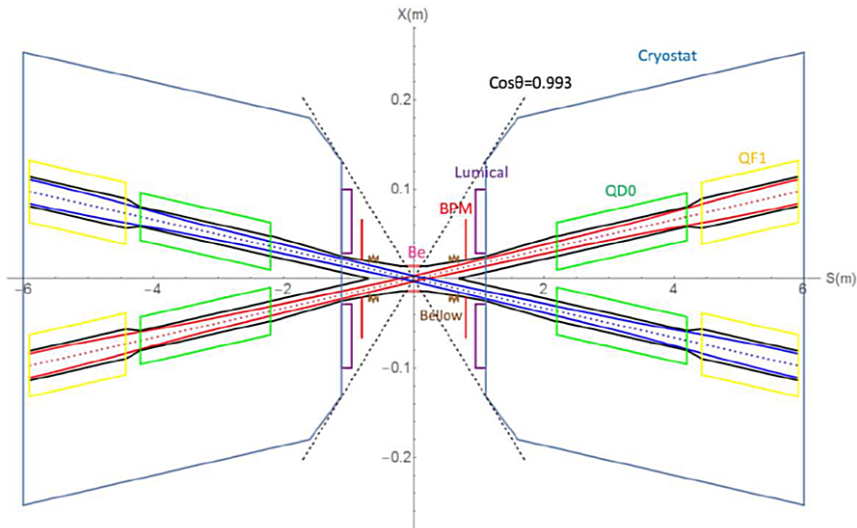


Fig. 1: Layout of the MDI region at CEPC.

The choice of technology of the luminometer at CEPC has not been finally determined yet. However, since this study is based on simulation of counting of low-angle Bhabha scattering without any other assumption but the angular acceptance of the luminometer, it is of no relevance for this study. If one would perform a more realistic simulation including detector response to signal and background, at least an energy cut on electron and positron tracks should be required to separate Bhabha events from the background. In such a case, effects like bias and resolution of energy measurement as well as the uncertainties from calibration of the luminometer should be included as additional sources of systematic uncertainty. The same happens if one includes other selection criteria based on polar and azimuthal angles of a Bhabha candidate.

3 Integrated luminosity measurement and systematic uncertainties

Integrated luminosity measurement is a counting experiment conventionally based on the low angle Bhabha scattering (LAB). It is defined as:

$$\mathcal{L} = \frac{N_{Bh}}{\sigma_{Bh}}, \quad (1)$$

where N_{Bh} is Bhabha count in the certain phase space of parameters and σ_{Bh} the SAB cross-section.

To control integrated luminosity at the required level of 10^{-4} at the Z^0 pole, both Bhabha count and theoretical cross-section should be known with the same precision. The Bhabha cross-section scales with the center-of-mass energy as [4]:

$$\frac{d\sigma}{d\theta} = \frac{2\pi\alpha_{em}^2}{s} \cdot \frac{\sin\theta}{\sin^4(\frac{\theta}{2})} \approx \frac{32\pi\alpha_{em}^2}{s} \cdot \frac{1}{\theta^3}, \quad (2)$$

where α_{em} is the QED constant and θ the polar angle of the emitted Bhabha particles. Uncertainty of 10^{-4} of the cross-section implies that the available center-of-mass energy should be known with $\Delta(\sqrt{s}) \leq 5$ MeV. There is an ongoing work at future Higgs factories [5] to check the feasibility of \sqrt{s} determination using di-muon production reconstructed in the central tracker.

As discussed in [6], many s-channel processes far from the resonance will have the same cross-section dependence on the center-of-mass energy, leading to effective cancellation of the uncertainties in the cross-section measurement. It is up to individual cross-section measurement analysis to determine if uncertainty of the integrated luminosity measurement caused by the uncertainty of \sqrt{s} is an issue.

Placement of the luminometer on the z-axis with the CEPC crossing angle of 33 mrad leads to the reduction in Bhabha count for $\sim 70\%$ in comparison to the count with the luminometer placed on the s-axis. Since the overall Bhabha count in 16 ab^{-1} of integrated luminosity expected at the Z^0 pole will be of order of 10^{12} for the detector placed on the s-axis, its displacement to the z-axis with the same luminometer apertures will contribute to the relative statistical uncertainty of the count as $1.2 \cdot 10^{-6}$. Hitmap in the first plane of the luminometer will look different, as can be seen on Fig. 2, with the expected loss of the axial symmetry.

Further we discuss feasibility and requirements for 10^{-4} precision of counting at the Z^0 pole, considering that each systematic effect individual contribution to the uncertainty of the integrated luminosity is of order of 10^{-4} . We have assumed event selection in polar angle acceptance to be asymmetric between the left and right arms of the detector. In [2], at the one side of the luminometer, the full fiducial volume is considered, while at the other side the inner radial acceptance is shrunken by 1 mm. In this study, the outer radial acceptance is also shrunken by 1 mm, as it has been done at OPAL. This has been done randomly to the left (L) and right (R) sides of the luminometer, on event by event basis. For symmetric

event selection we consider the full fiducial volumes of the both sides of luminometer. As will be discussed further, different detector positioning (s-axis and z-axis) interfere with a way of counting in a nontrivial way. Fig. 3 provides an illustrative depiction of the s- and z-axes configuration in collisions with the crossing angle.

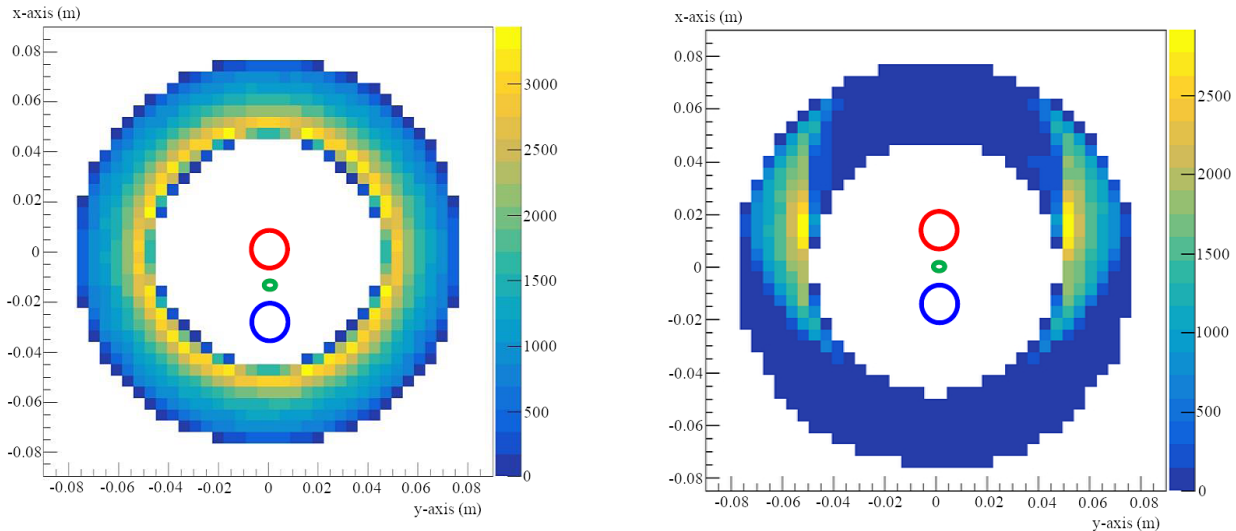


Fig. 2: Hitmap of the first plane of the luminometer placed around the outgoing beam (left) and z-axis (right). Red and blue circles represent the outgoing and incoming beam pipes respectively, and the green circle represents the z-axis.

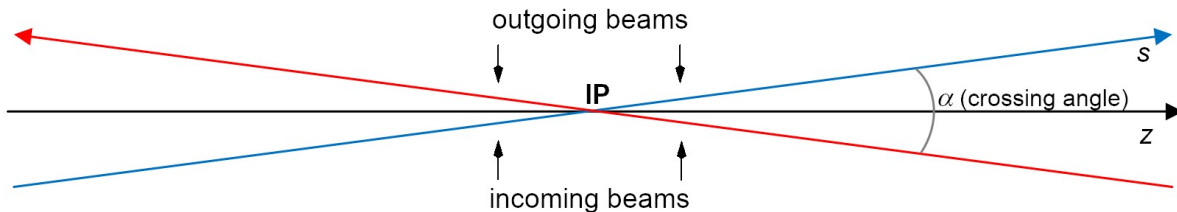


Fig. 3: Illustration of s-axis and z-axis.

3.1 Uncertainties from mechanics and positioning

Systematic uncertainties from detector and beam related uncertainties have been quantified through a simulation study, assuming $2 \cdot 10^7$ Bhabha scattering events generated using

BHLUMI V4.04 Bhabha event generator [7], at the Z^0 production threshold. Final state particles are generated in the polar angle range from 30 mrad to 100 mrad that is within a couple of mrad margin outside of the detector fiducial volume, to allow events with non-collinear final state radiation to contribute. Initial state radiation is also included. The effective Bhabha cross-section in this angular range is ~ 50 nb.

Considered detector-related uncertainties arising from manufacturing, positioning and alignment of the luminometer are:

- (1) Maximal uncertainty of the luminometer inner radius, Δr_{in} ,
- (2) RMS of the Gaussian spread of the measured radial shower position with respect to the true hit position, σ_r (i. e. by placing a tracker plane in front of the luminometer),
- (3) Maximal absolute uncertainty of the longitudinal distance between left and right halves of the luminometer, Δl , where both halves are shifted for $\pm \frac{\Delta l}{2}$ with respect to the interaction point,
- (4) RMS of the Gaussian distribution of mechanical fluctuations of the luminometer position with respect to the interaction point (IP), caused by vibrations and thermal stress, radial, $\sigma_{x_{IP}}$ and axial, $\sigma_{z_{IP}}$.

Considered deviations are maximal, as we assumed 10^{-4} contribution to the relative uncertainty of integrated luminosity from each individual effect. Figures 4-8 illustrate effects 1-4 respectively, for different ways of counting and different positions of the luminometer placed on the s- and z-axis. Limits of mechanical parameters are listed in table 1.

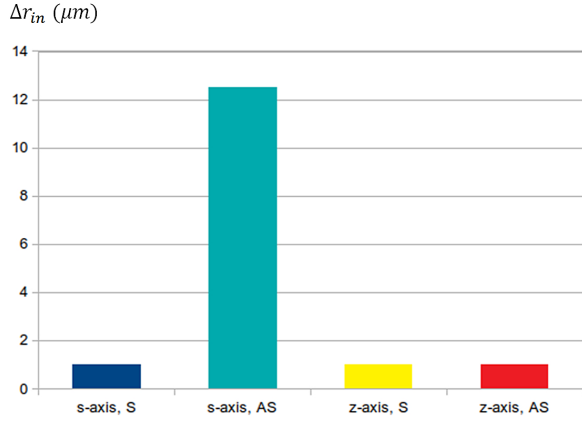
As can be seen from Figures 4(b)-8(b), for the detector placed at the z-axis asymmetric counting performs similarly as counting in the full fiducial volume and also similarly as asymmetric counting for the detector placed at the s-axis. With the detector placed at the s-axis the difference between the two ways of counting is quite significant, as illustrated in Figures 4(a)-8(a).

3.2 Beam related uncertainties

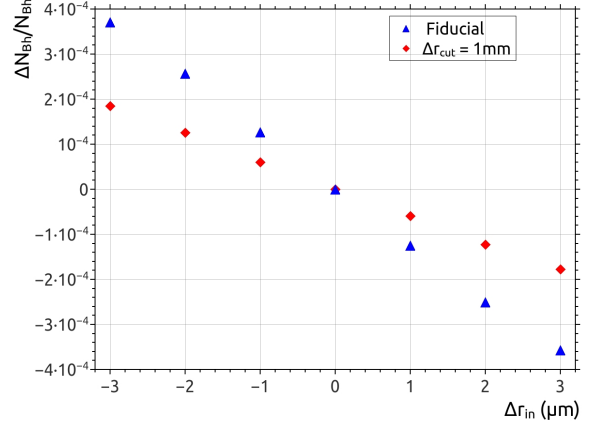
Several systematic uncertainties may arise from the uncertainties of beam properties and its delivery to the interaction point. The list of CEPC beam parameters addressed in this study is given in Table 1 [8].

Here we consider:

- (1) maximal permanent bias (ΔE) of a single beam energy with respect to the other beam, resulting in longitudinal boost of the incoming e^+e^- system with respect

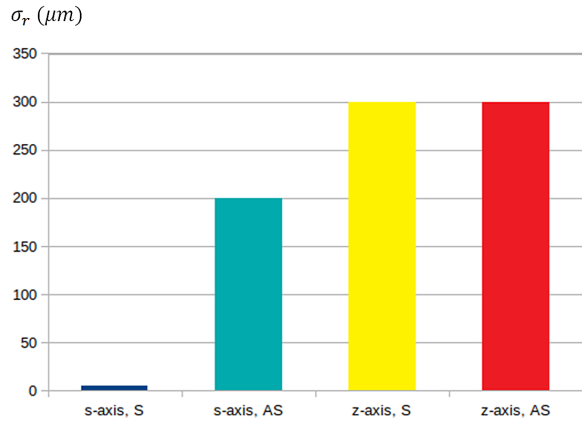


(a)

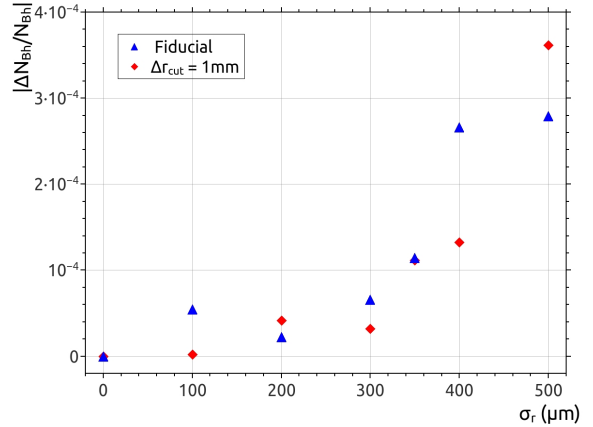


(b)

Fig. 4: (a) Variations of the inner aperture, Δr_{in} , for two different ways of counting: in the full fiducial volume (S) and the LEP-style (AS), for detector placed on the s- and z-axis; (b) Count uncertainty as a function of Δr_{in} for two different ways of counting (S-triangles, AS-diamonds), with the detector placed at the z-axis.

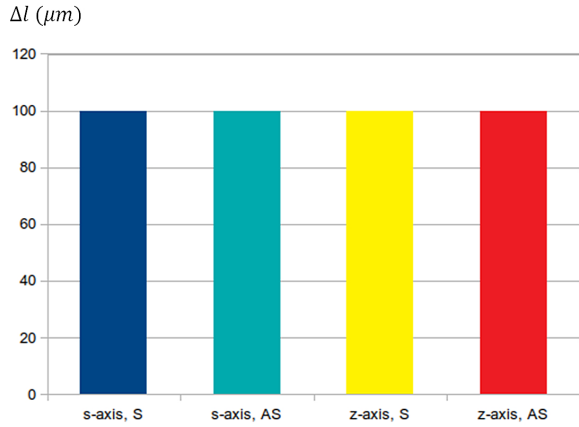


(a)

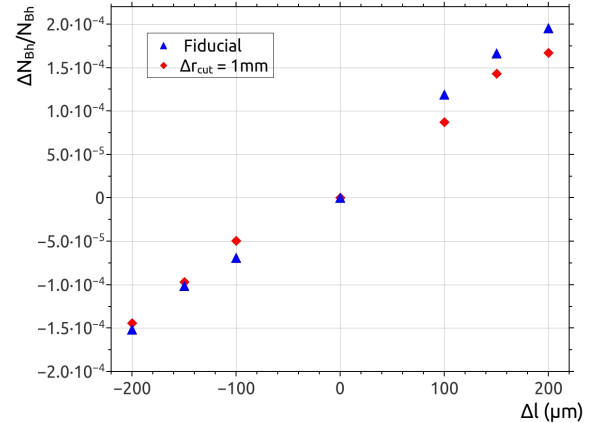


(b)

Fig. 5: (a) A comparison of results between the luminometer placed at the s-axis and luminometer placed at the z-axis for the RMS, of the Gaussian spread of the measured radial shower position with respect to the true impact position in the luminometer front plane, σ_r . (b) Count uncertainty as a function of σ_r for two different ways of counting (S-triangles, AS-diamonds), with the detector placed at the z-axis.

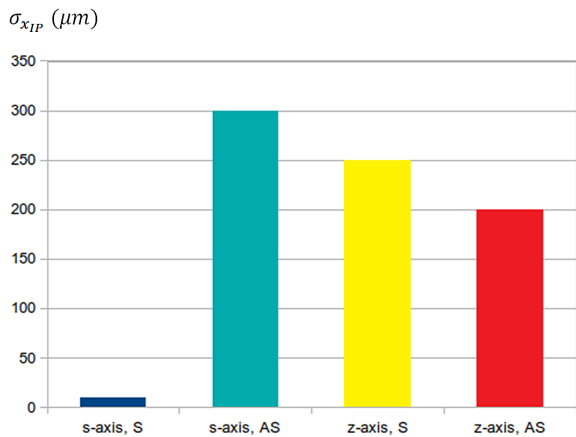


(a)

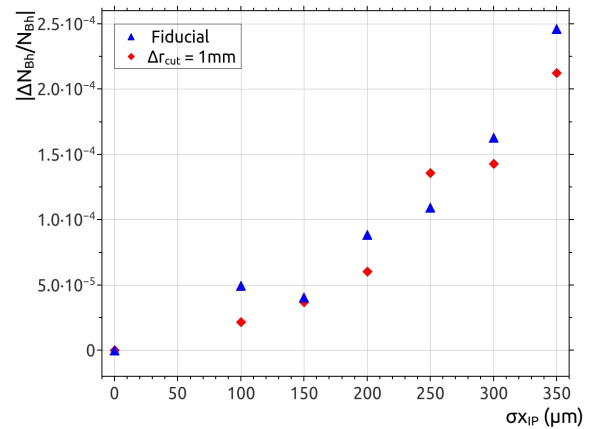


(b)

Fig. 6: (a) A comparison of results between the luminometer placed at the s-axis and luminometer placed at the z-axis for maximal absolute uncertainty, Δl , of the longitudinal distance between left and right halves of the luminometer; (b) Count uncertainty as a function of Δl for two different ways of counting (S-triangles, AS-diamonds), with the detector placed at the z-axis.



(a)



(b)

Fig. 7: (a) A comparison of results between the luminometer placed at the s-axis and luminometer placed at the z-axis for the RMS of the Gaussian distribution of mechanical fluctuations of the luminometer position with respect to the IP, caused by radial vibrations and thermal stress, $\sigma_{x_{IP}}$; (b) Count uncertainty as a function of $\sigma_{x_{IP}}$ for two different ways of counting (S-triangles, AS-diamonds), with the detector placed at the z-axis.

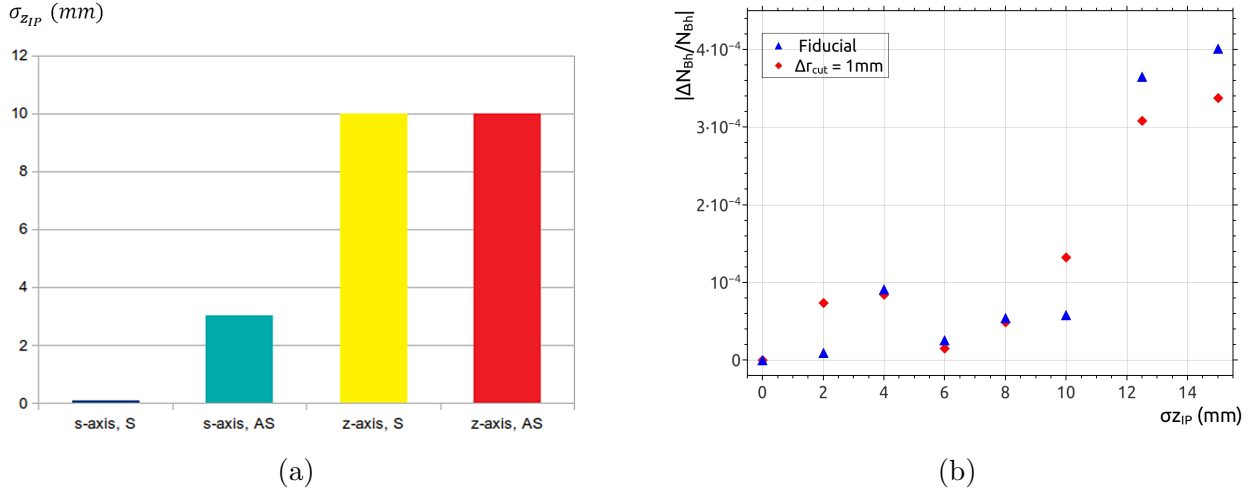


Fig. 8: (a) A comparison of results between the luminometer placed at the s-axis and luminometer placed at the z-axis for the RMS of the Gaussian distribution of mechanical fluctuations of the luminometer position with respect to the IP, caused by axial vibrations and thermal stress, $\sigma_{z_{IP}}$; (b) Count uncertainty as a function of $\sigma_{z_{IP}}$ for two different ways of counting (S-triangles, AS-diamonds), with the detector placed at the z-axis.

Table 1: CEPC TDR parameters at the Z^0 pole.

parameter	Z^0 pole
Half crossing angle at IP (mrad)	16.5
Energy (GeV)	45.5
Bunch population (10^{11})	1.4
Beam size at IP σ_x/σ_y ($\mu\text{m}/\text{nm}$)	6/35
Energy spread (natural) (%)	0.04
Luminosity per IP ($10^{34} \text{ cm}^{-2}\text{s}^{-1}$)	115

to the laboratory frame, and consequently, boost of the Bhabha center-of-mass system,

- (2) maximal half-width of the Gaussian of the beam energy spread ($\sigma_{E_{BS}}$), responsible for longitudinal boost on event-by-event basis, leading to the overall count loss of order of 10^{-4} ,
- (3) maximal radial (Δx_{IP}^{BS}) and axial (Δz_{IP}^{SY}) IP position displacements with respect to the luminometer, caused by the finite beam sizes (former) and beam synchronization (latter),

Table 2: Required minimal absolute precision of mechanical and beam parameters contributing to the relative uncertainty of the integrated luminosity of 10^{-4} at the Z^0 pole. The average net center-of-mass energy uncertainty ΔE_{CM} limit is derived by error propagation from the Bhabha cross-section dependence on the center-of-mass energy.

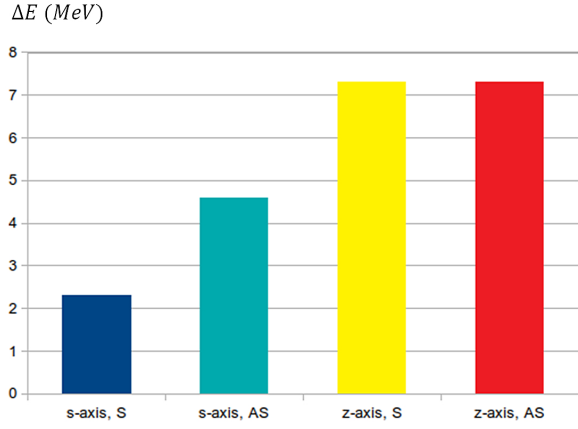
parameter	s-axis, symm.	s-axis, asymm.	z-axis, symm.	z-axis, asymm.
Δr_{in} (μm)	1	12	1	1
σ_r (μm)	5	200	300	300
Δl (μm)	100	100	100	100
$\sigma_{x_{IP}}$ (μm)	10	300	250	200
$\sigma_{z_{IP}}$ (mm)	0.08	3	10	10
ΔE_{CM} (MeV)	5	5	5	5
ΔE (MeV)	2	5	7	7
$\sigma_{E_{BS}}$ (MeV)	4	140	360	360
Δx_{IP}^{BS} (μm)	5	200	150	150
Δz_{IP}^{SY} (mm)	0.05	2	2	2
$\Delta\tau$ (ps)	0.08	3	3	3

- (4) maximal time shift in beam synchronization ($\Delta\tau_{SY}$), calculated from Δz_{IP}^{SY} , leading to the IP longitudinal displacement Δz_{IP}^{SY} .

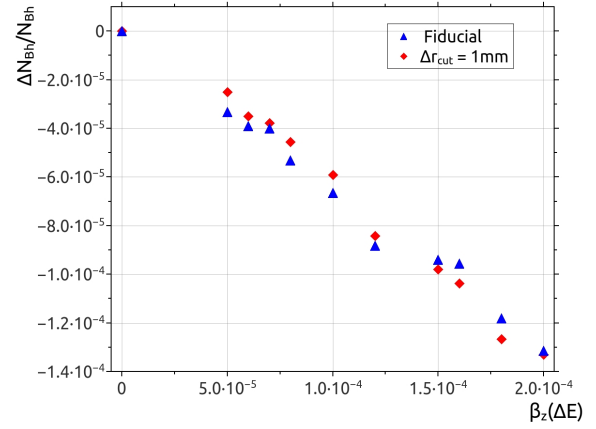
In the same manner as in the previous chapter, results for effects 1-3 are illustrated on Figures 9-12 and the upper limits are summarized in table 2, each contributing to the relative uncertainty of the integrated luminosity at the Z^0 pole as 10^{-4} .

As can be seen from Table 2, mechanical precision of the luminometer inner aperture is the major challenge, since the Bhabha cross-section is scaling with the polar angle as $\sigma \sim 1/\theta^3$.

The longitudinal boost of the Bhabha center-of-mass frame with respect to the laboratory frame (β_z) may be caused by any difference in beam energies, δE , in the form of bias ΔE of one beam with respect to the other, or as a random asymmetry caused by the beam energy spread ($\beta_z = 2 \cdot \delta E / \sqrt{s}$), or by the initial state radiation of beams (not considered here). Limits of ΔE and $\sigma_{E_{BS}}$ given in Table 2 are derived from Figures 9(b) and 10(b) and rounded with respect to statistical size of the sample. From Table 2 it can be seen that in terms of the beam-related parameters precision, displacement of the luminometer from the s-axis to the z-axis will not impact the luminosity precision, while some dependencies will be lost due to loss of spacial symmetries of Bhabha events.

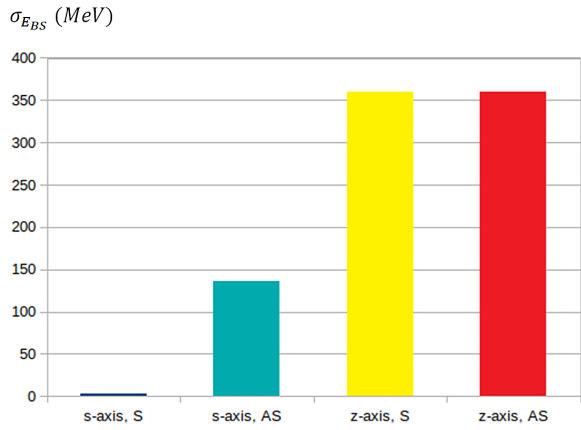


(a)

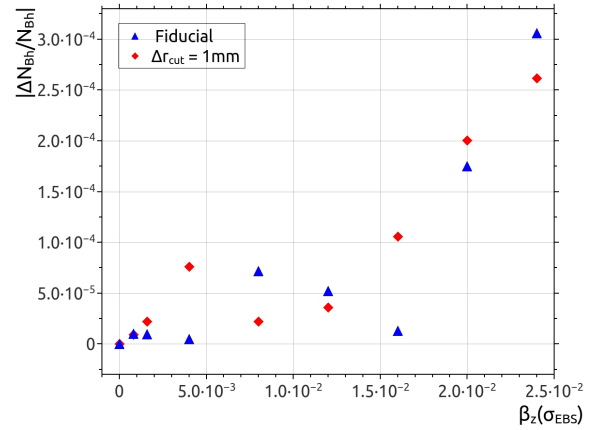


(b)

Fig. 9: (a) A comparison of results between the luminometer placed at the s-axis and luminometer placed at the z-axis for maximal bias of energy of one beam with respect to the other, ΔE ; (b) Loss of the Bhabha count in the luminometer due to the longitudinal boost of the center-of-mass frame, $\beta_z(\Delta E)$, for two different ways of counting (S-triangles, AS-diamonds), with the luminometer on the z-axis.

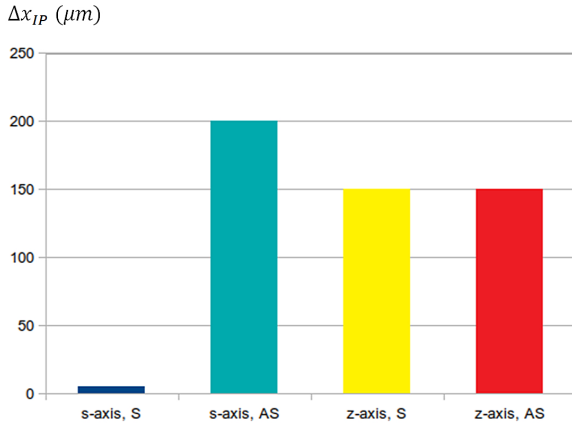


(a)

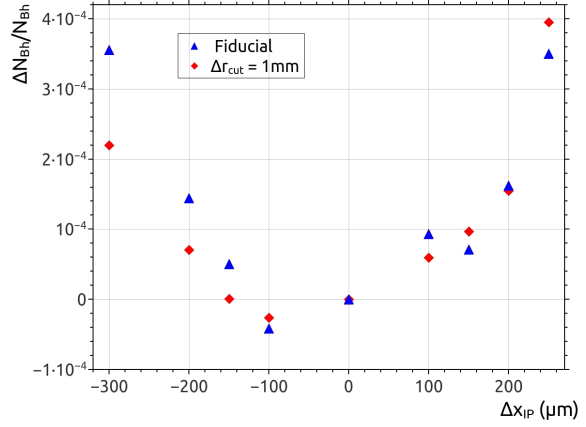


(b)

Fig. 10: (a) A comparison of results between the luminometer placed at the s-axis and luminometer placed at the z-axis for maximal half-width of the BES, corresponding to a relative statistical uncertainty of \mathcal{L} , σ_{EBS} ; (b) Loss of the Bhabha count in the luminometer due to longitudinal boost of the Bhabha center-of-mass frame caused by BES, $\beta_z(\sigma_{EBS})$, for two different ways of counting (S-triangles, AS-diamonds), with the luminometer on the z-axis.

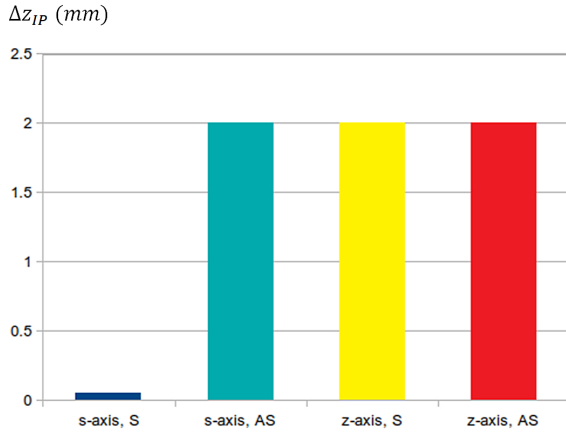


(a)

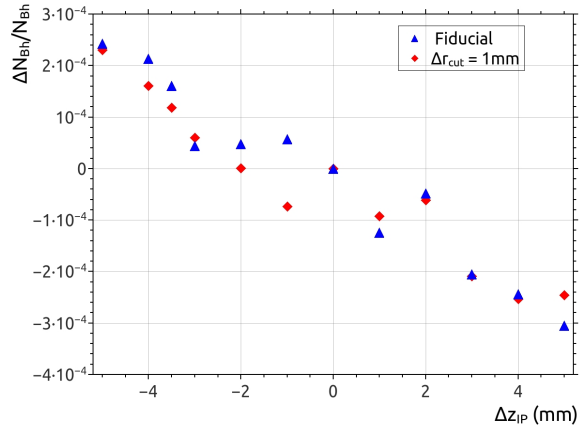


(b)

Fig. 11: (a) A comparison of results between the luminometer placed at the s-axis and luminometer placed at the z-axis for maximal radial IP position displacement with respect to the luminometer (Δx_{IP}^{BS}); (b) Count uncertainty as a function of Δx_{IP}^{BS} for two different ways of counting (S-triangles, AS-diamonds), with the detector placed at the z-axis.



(a)



(b)

Fig. 12: (a) A comparison of results between the luminometer placed at the s-axis and luminometer placed at the z-axis for maximal axial IP position displacements with respect to the luminometer (Δz_{IP}^{BS}); (b) Count uncertainty as a function of Δz_{IP}^{BS} for two different ways of counting (S-triangles, AS-diamonds), with the detector placed at the z-axis.

Due to hard precision requirement on luminometer inner aperture, as well as to numerous and sometimes complex systematic effects in integrated luminosity measurement, like the effects caused by beam-beam interactions [9], it is worth to explore, in addition, a possibility

to measure integrated luminosity with additional central processes, such as di-muon or di-photon production [10].

4 Conclusion

Although the method of integrated luminosity has already been studied in great detail at LEP, proposals for new e^+e^- colliders call for quantification of achievable luminosity precision in each individual case. We do it here for CEPC, from the perspective of mechanical and beam-related requirements at the Z^0 pole, with detector placed on the z-axis.

At the Z^0 pole, control of the luminometer inner radius at the micrometer level is posing the most demanding requirement regarding detector manufacturing, regardless of the luminometer's positioning (on the s-axis or on the z-axis). It is important to note that eventual changes in the luminometer design towards smaller polar angle coverage will require control of the luminometer inner radius even below micrometer precision, according to the dependence of the Bhabha cross-section on the polar angles of the scattered particles. However, these results are obtained under assumption that the change of the luminometer's inner radius corresponds to exactly the same change of the inner radius of the luminometer's fiducial volume, which needs to be approved. Also, control of the asymmetrical bias in beam energies might be challenging, while the beam energy spread can be relaxed significantly beyond the current half-width of 18 MeV at the Z^0 pole (0.04%, Table 1).

From the point of view of experimental input for the Bhabha cross-section calculations, center-of-mass energy should be known at the 10^{-4} level, which requires further studies in terms of feasibility of such a precision. This might be an issue for the cross-section measurements of the slope of a production threshold.

Although the simulated Bhabha samples are statistically small to be exact on boundaries of the considered systematics, distribution of central values presented in this study confirms that considering the mechanics and positioning, as well as the beam-related uncertainties, no effect seems to be more critical for precision measurement of the integrated luminosity if the luminometer is placed around the z-axis than if it is placed around the outgoing beams. The LEP-style asymmetric counting, however, will not be effective for the luminometer placed on the z-axis to cope with the effects affecting the left-right symmetry.

Complex metrology, together with the beam-related interactions affecting the Bhabha final state at small polar angles may call for consideration of an alternative central process, like di-muon or di-photon production for the integrated luminosity measurement, with hopefully less complex systematic effects subjected to further studies. In addition, studies presented here should be complemented with a full simulation study of systematic effects

arising from the detector design, technology and performance in the presence of realistic backgrounds.

Acknowledgment

This research was funded by the Ministry of Education, Science and Technological Development of the Republic of Serbia and by the Science Fund of the Republic of Serbia through the Grant No. 7699827, IDEJE HIGHTONE-P.

References

- [1] The CEPC Study Group, CEPC Conceptual Design Report: Volume 2 - Physics & Detector [arXiv:1811.10545 [hep-ex]] (2018). <https://doi.org/10.48550/arXiv.1811.10545>
- [2] I. Smiljanic et al., JINST **17** P09014 (2022). [10.1088/1748-0221/17/09/P09014](https://doi.org/10.1088/1748-0221/17/09/P09014)
- [3] G. Abbiendi et al. [OPAL Collaboration], Eur.Phys.J.C **14**, 373–425 (2000). <https://doi.org/10.1007/s100520000353>
- [4] H Abramowicz et al. [FCAL Collaboration], JINST **5** P12002 (2010). [10.1088/1748-0221/5/12/P12002](https://doi.org/10.1088/1748-0221/5/12/P12002)
- [5] G. Wilson, *Center-of-mass energy determination using dimuon events at ILC*, talk given at ILC Workshop on Potential Experiments (ILCX2021) (2021). https://agenda.linearcollider.org/event/9211/contributions/49276/attachments/37409/58737/ILCX_GWW_V3.pdf.
- [6] A. Stahl, LC-DET-2005-004 (2005). <https://bib-pubdb1.desy.de/record/587787/files/LC-DET-2005-004.pdf>
- [7] S. Jadach et al., Comput.Phys.Commun. **102**, 229–251 (1997). [https://doi.org/10.1016/S0010-4655\(96\)00156-7](https://doi.org/10.1016/S0010-4655(96)00156-7)
- [8] J. Gao, *CEPC Accelerator General Status Overview*, talk given at The 2023 International Workshop on CEPC (EU Edition) (2023). https://indico.ph.ed.ac.uk/event/259/contributions/2466/attachments/1305/1959/CEPC_Accelerator_General_Status_Overview-v1.pdf.
- [9] G. Voutsinas, E. Perez, M. Dam et al. J.High Energ.Phys. **225** (2019). [https://doi.org/10.1007/JHEP10\(2019\)225](https://doi.org/10.1007/JHEP10(2019)225)
- [10] J. de Blas et al. *Focus topics for the ECFA study on Higgs / Top / EW factories*, (2024)[arXiv:2401.07564 [hep-ph]]. <https://doi.org/10.48550/arXiv.2401.07564>